

Submesoscale potential vorticity

Christian Buckingham¹

¹Université de Bretagne Occidentale

November 24, 2022

Abstract

Ertel's potential vorticity theorem is essentially a clever combination of two conservation principles. The result is a conserved scalar q that accurately reflects vorticity values that fluid parcels can possess and acts as a tracer for fluid flow. While true at large horizontal scales in the ocean and atmosphere, at increasingly smaller scales and in sharply curved fronts, its accuracy breaks down. This is because Earth's rotation imparts angular momentum to fluid parcels and the conservation of absolute angular momentum L restricts the range of centripetal accelerations possible in balanced flow; this correspondingly restricts vorticity. To address this discrepancy, we revisit Ertel's derivation and obtain a new conserved scalar Lq that more properly reflects the vorticity of fluid parcels at these small horizontal scales. Although limited to flows on the f plane, this theorem nevertheless highlights a fundamental principle applicable to all geophysical fluids: at sufficiently small horizontal scales such that L can appropriately be conserved, centripetal accelerations-or curvature-can modify the vorticity of fluid parcels observed on the sphere.

Submesoscale potential vorticity

Journal:	<i>Journal of Fluid Mechanics</i>
Manuscript ID	JFM-21-1376
Manuscript Type:	JFM Papers
Date Submitted by the Author:	19-Aug-2021
Complete List of Authors:	Buckingham, Christian; Université de Bretagne Occidentale,
JFM Keywords:	Baroclinic flows < Geophysical and Geological Flows, Rotating flows < Geophysical and Geological Flows, Stratified flows < Geophysical and Geological Flows
Abstract:	<p>Ertel's potential vorticity theorem is essentially a clever combination of two conservation principles. The result is a conserved scalar q that accurately reflects vorticity values that fluid parcels can possess and acts as a tracer for fluid flow. While true at large horizontal scales in the ocean and atmosphere, at increasingly smaller scales and in sharply curved fronts, its accuracy breaks down. This is because Earth's rotation imparts angular momentum to fluid parcels and the conservation of absolute angular momentum L restricts the range of centripetal accelerations possible in balanced flow; this correspondingly restricts vorticity. To address this discrepancy, we revisit Ertel's derivation and obtain a new conserved scalar Lq that more properly reflects the vorticity of fluid parcels at these small horizontal scales. Although limited to flows on the f plane, this theorem nevertheless highlights a fundamental principle applicable to all geophysical fluids: at sufficiently small horizontal scales such that L can appropriately be defined, centripetal accelerations—or curvature—can modify the vorticity of fluid parcels observed on the sphere.</p>

SCHOLARONE™
Manuscripts

Banner appropriate to article type will appear here in typeset article

1 Submesoscale potential vorticity

2 **Christian E. Buckingham**¹†

3 ¹Université de Bretagne Occidentale, CNRS, IRD, Ifremer, Laboratoire d’Océanographie Physique et
4 Spatiale, IUEM, Rue Dumont d’Urville, 29280, Plouzané, FR

5 ²British Antarctic Survey, Cambridge, CB3 0ET, UK

6 (Received xx; revised xx; accepted xx)

7 Ertel’s potential vorticity theorem is essentially a clever combination of two conservation
8 principles. The result is a conserved scalar q that accurately reflects vorticity values that fluid
9 parcels can possess and acts as a tracer for fluid flow. While true at large horizontal scales
10 in the ocean and atmosphere, at increasingly smaller scales and in sharply curved fronts,
11 its accuracy breaks down. This is because Earth’s rotation imparts angular momentum to
12 fluid parcels and the conservation of absolute angular momentum L restricts the range of
13 centripetal accelerations possible in balanced flow; this correspondingly restricts vorticity.
14 To address this discrepancy, we revisit Ertel’s derivation and obtain a new conserved scalar
15 Lq that more properly reflects the vorticity of fluid parcels at these small horizontal scales.
16 Although limited to flows on the f plane, this theorem nevertheless highlights a fundamental
17 principle applicable to all geophysical fluids: at sufficiently small horizontal scales such
18 that L can appropriately be defined, centripetal accelerations—or curvature—can modify the
19 vorticity of fluid parcels observed on the sphere.

20 **Key words:** These will be chosen by the author during the online submission process and
21 will then be added during the typesetting process (see [Keyword PDF](#) for the full list). Other
22 classifications will be added at the same time.

23 **MSC Codes** (*Optional*)

24 1. Introduction

25 Ocean dynamics at small horizontal scales have garnered considerable attention in recent
26 years. This attention has been evident in both *observational* and *modelling* sectors of the
27 physical oceanographic community. New advancements in observing systems—including
28 those from autonomous floats (D’Asaro *et al.* 2011), gliders (Thompson *et al.* 2016; du Plessis
29 *et al.* 2019), and long-range surface vehicles such as SailDrones (Gentemann *et al.* 2020)—
30 have increased our capability to resolve small-scale phenomena. One result is that gradients
31 in velocity and density at horizontal scales between 1 and 10 km—previously only inferred

† Email address for correspondence: christian.buckingham@gmail.com

2

32 from spacecraft (*e.g.* Flament *et al.* 1985; Scully-Power 1986; Munk *et al.* 2000) and long-
 33 term moored measurements (*e.g.* Bane *et al.* 1989; Lilly & Rhines 2002; Buckingham *et al.*
 34 2016)—are now resolved or becoming resolved in targeted process studies (*e.g.* Thomas
 35 & Lee 2005; D’Asaro *et al.* 2011; Shcherbina *et al.* 2013; Thomas *et al.* 2013; Adams
 36 *et al.* 2017; Naveira Garabato *et al.* 2019). At the same time, computational resources
 37 have increased at an unimaginable rate, permitting scientists the ability to realistically
 38 simulate dynamics at such fine scales in numerical models. At present, models are capable
 39 of providing realistic ocean simulations within nested, regional configurations, horizontal
 40 grid resolutions of 100 m are possible (Onken *et al.* 2020), with the result that oceanic
 41 phenomena with e -folding scales of several hundred meters can be resolved. These same
 42 simulations run on the globe produce simulations at horizontal resolutions approaching 1 km
 43 (<https://data.nas.nasa.gov/ecco/data.php>).

44 Oceanic flows at these small spatial scales are commonly referred to as *submesoscale*
 45 *processes* (Thomas *et al.* 2008; McWilliams 2016) in order to distinguish them from
 46 larger-scale counter-parts, referred to as *mesoscale processes*. At mid-latitudes, these terms
 47 correspond to horizontal scales smaller than 10 km (submesoscale) and larger than 30 km
 48 (mesoscale), where the transition between these scales is roughly equal to the first-mode,
 49 baroclinic deformation radius R_d (Chelton *et al.* 1998; Smith 2007). It is notable that at
 50 high latitudes, R_d approaches 1-10 km (Timmermans *et al.* 2008; Nurser & Bacon 2014)
 51 such that assigning absolute scales to these phenomena is problematic. This has motivated a
 52 dynamical definition (Thomas *et al.* 2008; McWilliams 2016).

53 1.1. A dynamical definition of the oceanic submesoscale

54 Processes within the oceanic submesoscale regime are typically characterized by enhanced
 55 gradients in velocity and density. In particular, the vertical component of relative vorticity
 56 $\zeta = (\nabla \times \mathbf{u}) \cdot \hat{\mathbf{k}}$ rivals the vertical component of planetary vorticity $f = 2\boldsymbol{\Omega} \cdot \hat{\mathbf{k}} = 2\Omega \sin \theta$
 57 and, as a consequence of thermal wind balance (TWB), $\partial_z \mathbf{u}_h = \frac{1}{f} \hat{\mathbf{k}} \times \nabla_h b$, pronounced
 58 horizontal density gradients imply enhanced vertical shears. Finally, mixing is typically
 59 enhanced within boundary layers, such that vertical stratification N^2 is reduced. As a
 60 consequence, both gradient Rossby number ($Ro = \zeta/f$) and gradient Richardson number
 61 ($Ri = N^2/|\partial_z \mathbf{u}_h|^2$) have values which approach 1.0 within the oceanic submesoscale regime
 62 (Thomas *et al.* 2008; McWilliams 2016).

63 1.2. Broadening this definition to accommodate vortex flow

64 It is common to assume that the mean flow within fronts is in geostrophic and hydrostatic
 65 balance—*i.e.* TWB mentioned above. In Cartesian coordinates oriented relative to the front,
 66 we can write this as $f \partial_z \bar{v} = \partial_x \bar{b}$, where $M^2 = \partial_x \bar{b}$ denotes the mean cross-frontal buoyancy
 67 gradient. In these expressions, \mathbf{u}_h is the horizontal velocity, \bar{v} denotes the mean velocity in
 68 the along-front direction, $\partial_z \bar{v}$ is the mean vertical shear, $b = -g\rho/\rho_o$ denotes buoyancy (g
 69 is gravity, ρ is density, and ρ_o is a reference density), and x and y are cross-front and along-
 70 front coordinates, respectively. This is a reasonable approximation for density fronts with
 71 horizontal scales larger than R_d (Pedlosky 1987). However, at increasingly smaller scales,
 72 the momentum balance can shift from a geostrophic to cyclogeostrophic balance, reflecting
 73 the growing importance of centripetal accelerations. Together with the hydrostatic balance,
 74 this implies a gradient wind balance (GWB):

$$75 \quad (f + 2\bar{v}/r) \partial_z \bar{v} = \partial_r \bar{b} \quad (1.1)$$

76 Factoring out the Coriolis parameter from the quantity in parentheses immediately leads
 77 to a nondimensional parameter which quantifies the impact of centripetal accelerations on

78 the vertical shear, the curvature number: $Cu = 2\bar{v}/(fr)$. This nondimensional number also
 79 scales with the ratio of centripetal to Coriolis accelerations (Shakespeare 2016). In the
 80 expression above, r denotes the cross-front coordinate, such that $M^2 = \partial_r \bar{b}$ is the radial
 81 gradient buoyancy gradient and implicitly contains information regarding frontal curvature.
 82 For clarity, note that $Cu > 0$ for cyclonic curved fronts and $Cu < 0$ negative for anticyclonic
 83 curved fronts. (In vortices, r is the distance from the vortex center, while $\bar{v} > 0$ for cyclones
 84 and $\bar{v} < 0$ for anticyclones. In meandering baroclinic frontal flows, we can replace r with a
 85 local radius of curvature R . Since the along-front flow is $\bar{v} > 0$, R must be signed.) Moreover,
 86 in the limit $Cu \rightarrow 0$ one recovers TWB. GWB is therefore descriptive of highly curved fronts
 87 and vortices and includes TWB as a limiting case. We therefore broaden the definition of
 88 the oceanic submesoscale as being a regime in which the mean flow is in GWB, and where
 89 gradient Rossby, Richardson, and curvature numbers (Ro , Ri , Cu) can be of order-one.

90 1.3. Observations of relative vorticity at kilometer-scales

91 It is broadly understood that the distribution of relative vorticity as measured at submesoscale
 92 (*i.e.* 1-10 km) resolutions in the oceans has two limiting characteristics. First, the distribution
 93 of Ro is predominantly cyclonic (positively skewed) for frontal flows and predominantly
 94 anticyclonic (negatively skewed) for eddying or vortex flows (Figure 1). By “vortex flow,” we
 95 include both highly curved fronts and coherent vortices. This has been noted, for example,
 96 in the upper ocean observations (Rudnick 2001; Shcherbina *et al.* 2013; Buckingham *et al.*
 97 2016) and model simulations (Roulet & Klein 2010; Shcherbina *et al.* 2013). Away from the
 98 upper ocean, the cyclone-anticyclone asymmetry has been documented in float trajectories,
 99 vertical hydrographic profiles, and moored measurements (*e.g.* McDowell & Rossby 1978;
 100 Riser *et al.* 1986; D’Asaro 1988; Bane *et al.* 1989; Zhao *et al.* 2014), but here the statistics
 101 are more limited.

102 To aid in our discussions, we reproduce in Figure 1 the joint probability density function
 103 (PDF) of vorticity ζ and strain rate $\alpha = [(\partial_x u - \partial_y v)^2 + (\partial_x v + \partial_y u)^2]^{1/2}$ as documented
 104 by (Shcherbina *et al.* 2013, Figure 5). As vorticity increases, the joint PDF approaches a
 105 pure shear relationship and is unbounded ($\zeta \approx \alpha$), indicative of fronts. By contrast, as
 106 vorticity decreases (becomes more negative), the negative vorticity is bounded, with a higher
 107 probability of solid-body rotation ($\zeta \gg \alpha$), indicative of vortex flow. While the unbounded
 108 nature of cyclonic vorticity associated with straight fronts can be rationalized in terms of
 109 potential vorticity (PV) conservation (Hoskins & Bretherton 1972)[†], the increased likelihood
 110 of anticyclonic vorticity associated with vortex flow has not fully been explained. In this study,
 111 we provide an explanation for this characteristic.

112 1.4. Motivation and outline of the study

113 In a previous study (Buckingham *et al.* 2020a,b), it was suggested that a unique conservation
 114 principle may be present within highly curved fronts and vortices (hereafter “vortex flow”)
 115 on the f -plane. Moreover, this principle was invoked when proposing a mechanism for the
 116 evolution of small-scale (*i.e.* submesoscale and polar mesoscale) vortices in the ocean. The
 117 implication was that fluid parcels within curved baroclinic fronts and vortices do not simply
 118 conserve the Ertel PV (Ertel 1942), and therefore undergo vortex stretching and tilting to

[†] It helps to think of this in the barotropic limit, for which the equation for the evolution of vorticity is $D\zeta/Dt = (f + \zeta)\partial_z w - \beta v$, where v is meridional velocity, w is vertical velocity, and $\beta = df/dy$. Letting $\beta = 0$, dynamically, what occurs is that as a fluid parcel is stretched ($\partial_z w > 0$), it spins up cyclonically without bound. As this same fluid parcel is compressed ($\partial_z w < 0$), it spins in an opposite direction. However, this motion is bounded since $D\zeta/Dt$ becomes increasingly smaller as ζ approaches $-f$. In non-dimensional form, we find that $Ro > -1$. In the baroclinic limit, other constraints (*i.e.* on density) become important and modify this lower bound. In particular, the bound is $Ro > -1 + Ri^{-1}$.

4

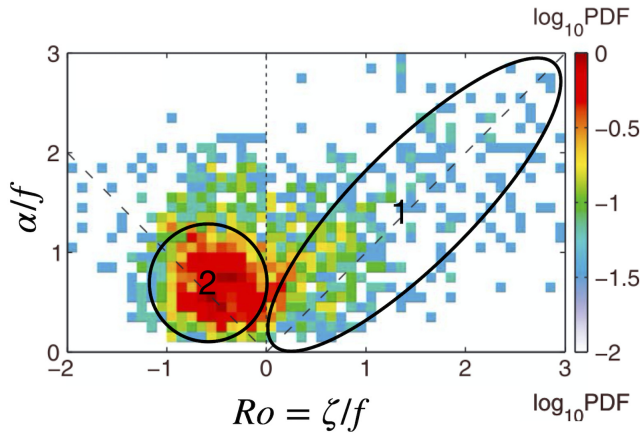


Figure 1: The joint PDF of relative vorticity ζ and magnitude strain rate α normalized by the Coriolis parameter f as documented in observations in the vicinity of the Gulf Stream; adapted from Shcherbina *et al.* (2013, Figure 5a). Two regimes are identified: (1) cyclonic vorticity that approaches the strain rate α with increasing vorticity (indicative of straight fronts) and (2) anticyclonic vorticity that is bounded in $Ro = \zeta/f$ (indicative of vortex flow). The unbounded nature of cyclonic vorticity can be explained using PV conservation at a geostrophic front, while the peak associated with anticyclonic vortex flow can be explained using Lq conservation.

119 conserve this quantity. Rather, fluid parcels adjust barotropic and baroclinic components of
 120 another scalar, \ddagger which is proportional to the product of the Ertel PV (q) and the vertical
 121 component of absolute angular momentum (L). If true, the fact that this additional term L
 122 enters the conserved quantity provides an added constraint to the problem, making inviscid,
 123 adiabatic motions within highly curved baroclinic flows differ from those in which PV alone
 124 is the conserved scalar. As is demonstrated below, this places constraints on relative vorticity
 125 and may help to explain the characteristic of vorticity just described (cf. Figure 1). A key
 126 assumption is continuity of the fluid in the direction of the mean flow at radius r such that
 127 L can be appropriately defined (Rayleigh 1917; Shakespeare 2016). In the oceans, at scales
 128 dynamically described as “submesoscale” (*e.g.* horizontal scales 1–10 km) this is possible.

129 The purpose of this manuscript is three-fold. First, we wish to provide a rational argument
 130 for the statement that “the product of the absolute angular momentum and Ertel PV is
 131 conserved following fluid parcels.” Second, we wish to assess under which conditions such
 132 a statement is true. Third, we seek to fully explain above feature within the distributions of
 133 relative vorticity. In doing so, we indirectly lay a more formal foundation for the analysis of
 134 flows in which centrifugal forces are present.

135 The outline of the study is as follows. We first derive a conservation equation for the new
 136 scalar quantity Lq (section 2). This derivation follows that of Ertel (1942) but includes a
 137 presentation of absolute angular momentum, a topic neglected in most oceanographic studies.
 138 Application of the theorem to oceanic flows is discussed in section 3 and its limitations are
 139 described in section 4. The study concludes in section 5.

\ddagger Buckingham *et al.* (2020a,b) suggested that the generalized Rayleigh discriminant $\Phi = 2Lq/r^2$ was conserved following fluid parcels in highly curved fronts and vortices. However, as demonstrated below, this statement is incorrect: it is Lq or $r^2\Phi$ that is conserved following fluid parcels. This difference is critical because it implies cross-frontal motion will modify the stability “seen” by fluid parcels.

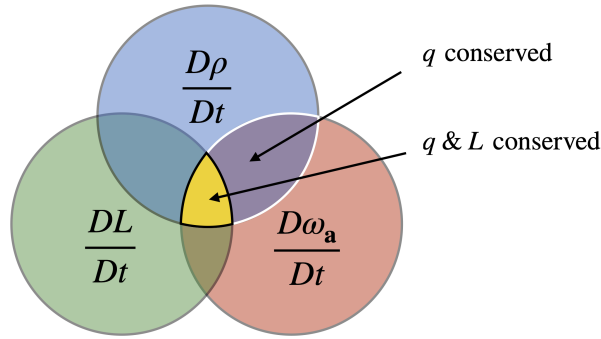


Figure 2: A Venn diagram conceptually depicting the intersection of three conservation principles: absolute vorticity ω_a , density ρ , and the vertical component of absolute angular momentum L . Ertel (1942) focused on the intersection of density and vorticity conservation. This study examines a subset of such flows for which both PV q and absolute angular momentum L can be conserved (*i.e.* vortex flow).

140 2. Derivation

141 Ertel's (1942) PV theorem is a clever combination of two independent conservation
 142 principles, each with its conditions. It is therefore logical to presume that the inclusion
 143 of a third conservation principle together with its corresponding conditions could permit a
 144 new vorticity theorem subject to these additional limitations. This is illustrated conceptually
 145 in Figure 2.

146 2.1. Governing equations

147 The equations of motion describing the balance of forces per unit mass of a fluid parcel within
 148 a rotating reference frame are (Batchelor 1967; Pedlosky 1987; Cushman-Roisin 1994)

$$149 \quad \frac{D\mathbf{u}}{Dt} + 2\boldsymbol{\Omega} \times \mathbf{u} = -\frac{1}{\rho} \nabla p + \underbrace{\mathbf{g}^* + \mathbf{a}_c}_{\mathbf{g}} + \frac{\mathcal{F}}{\rho}, \quad (2.1)$$

150 where it is understood that all terms are evaluated within the rotating reference frame. Here,
 151 $D/Dt = \partial_t + \mathbf{u} \cdot \nabla \mathbf{u}$ denotes the material or substantial derivative, \mathbf{r} is the position vector,
 152 $\boldsymbol{\Omega}$ is the angular rotation rate ($|\boldsymbol{\Omega}| = 2\pi/\text{day} \approx 7.22 \times 10^{-5} \text{ s}^{-1}$ for Earth) and assumed
 153 to be constant, $2\boldsymbol{\Omega} \times \mathbf{u}$ is the Coriolis acceleration, $\mathbf{a}_c = -\boldsymbol{\Omega} \times (\boldsymbol{\Omega} \times \mathbf{r}) = |\boldsymbol{\Omega}|^2 \mathbf{r}_\perp$ is the
 154 centrifugal acceleration due to the rotation of the reference frame, ρ is density, p is pressure,
 155 \mathbf{g}^* is the acceleration due to gravity, and \mathcal{F} denotes the frictional force. It is customary to
 156 combine centrifugal and gravitational accelerations into a resultant acceleration $\mathbf{g} = \mathbf{g}^* + \mathbf{a}_c$,
 157 or *effective gravity*. The resultant is then approximately perpendicular to geopotential surfaces
 158 and, hence, oriented vertically[†] (Cushman-Roisin 1994). For clarity, we illustrate planetary
 159 vorticity, gravitational acceleration, gravity, and centrifugal acceleration vectors (Figure 3).
 160

Mass conservation is given by the continuity equation

$$161 \quad \frac{\partial \rho}{\partial t} + \nabla \cdot (\rho \mathbf{u}) = 0. \quad (2.2)$$

162 An equation of state is typically necessary to relate ρ to known or measured variables. In the
 163 ocean, this is a complex function of temperature, salinity, and pressure. For simplicity in the
 164 present work, we assume we know the density perfectly.

[†] Local changes to the gravitational potential, for example, due to irregular topography or seamounts, will perturb \mathbf{g}^* from its mean direction.

6

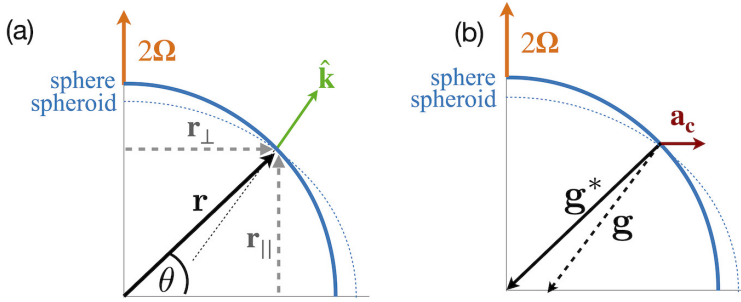


Figure 3: Illustration of vectors present within the equations of motion on the sphere (cf. Equation 2.1) and f -plane approximation (cf. Equation 2.3). In (a), we depict planetary vorticity 2Ω (orange), the position vector \mathbf{r} (heavy black), components of the position vector \mathbf{r}_\perp and \mathbf{r}_\parallel (gray), and vertical unit vector $\hat{\mathbf{k}}$ (green). In (b), we depict the gravitational vector \mathbf{g}^* (black), the centrifugal acceleration vector $\mathbf{a}_c = -\Omega \times (\Omega \times \mathbf{r}) = |\Omega|^2 \mathbf{r}_\perp$ (red), and the vector resultant, or effective gravity $\mathbf{g} = \mathbf{g}^* + \mathbf{a}_c$ (dashed black). We also illustrate the surface of Earth as represented by a sphere (solid blue) and oblate spheroid (dashed blue). The unit vector $\hat{\mathbf{k}}$ is anti-parallel to \mathbf{g} and, therefore, approximately perpendicular to the surface of the oblate spheroid.

165 *The f -plane approximation: rational and self-consistent*

166 The corresponding equations of motion valid under the f plane approximation are obtained
 167 by expressing Equation 2.1 in spherical coordinates, scaling the equations of motion, and
 168 discarding terms multiplied by $\delta = |ds|/R_e \ll 1$ or smaller, where $|ds| = R_e d\theta$ denotes a
 169 meridional arc length and R_e is the mean radius of Earth (Grimshaw 1975). The result is a
 170 vectorized set of equations comparable to Equation 2.1 except where $2\Omega \times \mathbf{u}$ is evaluated at
 171 a specific latitude θ_o :

$$172 \quad \frac{D\mathbf{u}}{Dt} + 2\mathbf{\Omega}_o \times \mathbf{u} = -\frac{1}{\rho} \nabla p + \mathbf{g} + \frac{\mathcal{F}}{\rho}. \quad (2.3)$$

173 In the cylindrical coordinate system, where the triad of orthogonal unit vectors $(\hat{\mathbf{r}}, \hat{\boldsymbol{\phi}}, \hat{\mathbf{k}})$
 174 point in radial, azimuthal, and vertical (upward) directions, respectively, the position
 175 vector is denoted by $\mathbf{r}_c = (r, \phi, z)$ and velocity by $\mathbf{u} = (u, v, w)$ (Figure 4). The material
 176 derivative is then $D/Dt = \partial_t + \mathbf{u} \cdot \nabla = \partial_t + u\partial_r + (v/r)\partial_\phi + w\partial_z$. Finally, the frictional force
 177 is $\mathcal{F} = (F_r, F_\phi, F_z)$ and effective gravity is $\mathbf{g} = (0, 0, -g)$. The choice of a cylindrical
 178 coordinate system on the f plane slightly complicates expression of planetary vorticity
 179 $2\mathbf{\Omega}_o$ owing to its variation with azimuth angle ϕ . Defining ϕ with respect to east, we have
 180 $2\mathbf{\Omega}_o = (0, 2|\Omega| \cos \theta_o \sin \phi, 2|\Omega| \sin \theta_o) = (0, \tilde{f}, f)$. To retain generality in our derivation
 181 below, we use Equation 2.3 together with the full Coriolis vector $\mathbf{\Omega}_o$. Note, Equation 2.2
 182 remains unaltered under the f plane approximation. Additionally, the position vectors in the
 183 spherical and cylindrical coordinate systems are related by $\mathbf{r} = \mathbf{r}_o + \mathbf{r}_c$, where \mathbf{r}_o denotes the
 184 origin of the cylindrical system at latitude θ_o (Figure 4).

185 Equation 2.3 is rational in that it follows logically from the spherical equations in the limit
 186 of small arc length. Moreover, as pointed out by Grimshaw (1975), the equation is also *self-*
 187 *consistent*; it possesses certain mathematical properties—*e.g.* differentiation is commutative—
 188 that permit subsequent derivations of vorticity, Ertel's PV theorem, etc. to be equivalent to
 189 those in spherical coordinates subject to these limiting conditions. This self-consistency is
 190 an important aspect of the derivation as it enables us to write a conservation equation for the
 191 absolute angular momentum that properly reflects dynamics on the oblate sphere. In contrast,

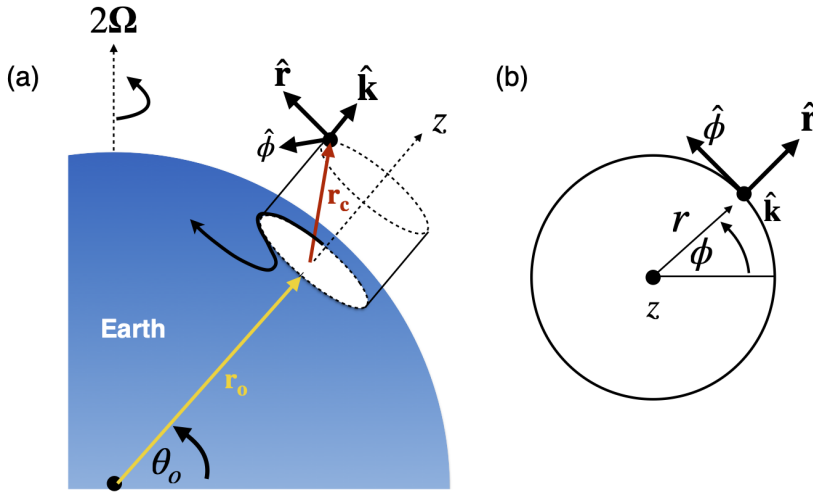


Figure 4: A cylindrical coordinate system on an f -plane at latitude $\theta = \theta_o$: (a) perspective view and (b) plan view, illustrating the orthogonal unit basis $(\hat{r}, \hat{\phi}, \hat{k})$, position vector $\mathbf{r}_c = (r, \phi, z)$ (red), where the angle ϕ is defined relative to an eastward direction, and a vector \mathbf{r}_o (yellow) which helps define the origin of the cylindrical coordinate system. Although not shown, the velocity is $\mathbf{u} = (u, v, w)$ and its components point in \hat{r} , $\hat{\phi}$, and \hat{k} directions, respectively.

192 the equations of motion under the β -plane approximation are not self-consistent (Grimshaw
193 1975) and may introduce dynamics not encountered on the sphere.

194 2.2. Absolute vorticity

195 Starting with the equations of motion, one can derive a conservation equation for absolute
196 vorticity (Batchelor 1967; Pedlosky 1987; Müller 1995). We first re-express Equation 2.3 in
197 terms of absolute vorticity $\boldsymbol{\omega}_a = \nabla \times \mathbf{u}_a = 2\boldsymbol{\Omega}_o + \nabla \times \mathbf{u} = 2\boldsymbol{\Omega}_o + \boldsymbol{\omega}$ (Batchelor 1967):

$$198 \quad \frac{\partial \mathbf{u}}{\partial t} + \boldsymbol{\omega}_a \times \mathbf{u} = -\frac{1}{\rho} \nabla p + \nabla [\mathbf{g} \cdot \mathbf{r}_c - (\mathbf{u} \cdot \mathbf{u})/2] + \frac{\mathcal{F}}{\rho}, \quad (2.4)$$

199 where $\mathbf{u}_a = \mathbf{u} + \boldsymbol{\Omega} \times \mathbf{r}_c$ is absolute velocity. Taking the curl of Equation 2.4 gives

$$200 \quad \frac{\partial \boldsymbol{\omega}}{\partial t} + \nabla \times (\boldsymbol{\omega}_a \times \mathbf{u}) = \frac{\nabla \rho \times \nabla p}{\rho^2} + \nabla \times \left(\frac{\mathcal{F}}{\rho} \right). \quad (2.5)$$

201 Using $\nabla \times (\mathbf{A} \times \mathbf{B}) = \mathbf{A} \nabla \cdot \mathbf{B} + (\mathbf{B} \cdot \nabla) \mathbf{A} - \mathbf{B} \nabla \cdot \mathbf{A} - (\mathbf{A} \cdot \nabla) \mathbf{B}$ (e.g. Riley *et al.* 2006),
202 noting that the planetary vorticity is constant,[†] and using the continuity equation (cf. Equa-
203 tion 2.2), we obtain a conservation equation for the absolute vorticity *per unit mass*:

$$204 \quad \frac{D}{Dt} \left(\frac{\boldsymbol{\omega}_a}{\rho} \right) = \left(\frac{\boldsymbol{\omega}_a}{\rho} \cdot \nabla \right) \mathbf{u} + \frac{\nabla \rho \times \nabla p}{\rho^3} + \left(\nabla \times \frac{\mathcal{F}}{\rho} \right) \frac{1}{\rho}. \quad (2.6)$$

205 Here, the divergence term $\boldsymbol{\omega}_a \nabla \cdot \mathbf{u}$ has been eliminated from the right-hand-side (RHS) by
206 including density within the material derivative on the left-hand-side (LHS).

[†] This is true regardless of the chosen coordinate system since, ignoring the precession of Earth's rotation axis, the vector $2\boldsymbol{\Omega}$ is unchanged.

8

2.3. Density or buoyancy (i.e. a thermodynamic variable)

207

208 Here, we follow Pedlosky (1987) (Ertel assumes $D\rho/Dt = 0$) and write the conservation of
209 a scalar λ as

$$210 \quad D\lambda/Dt = \frac{\partial\lambda}{\partial t} + \mathbf{u} \cdot \nabla\lambda = \Psi. \quad (2.7)$$

211 Taking the inner product of $\nabla\lambda$ and Equation 2.6, one obtains

$$212 \quad \nabla\lambda \cdot \frac{D}{Dt} \left(\frac{\boldsymbol{\omega}_a}{\rho} \right) = \nabla\lambda \cdot \left[\left(\frac{\boldsymbol{\omega}_a}{\rho} \cdot \nabla \right) \mathbf{u} \right] + \nabla\lambda \cdot \frac{\nabla\rho \times \nabla p}{\rho^3} + \frac{\nabla\lambda}{\rho} \cdot \left(\nabla \times \frac{\mathcal{F}}{\rho} \right). \quad (2.8)$$

213 Incorporating $\nabla\lambda$ into the material derivative on the LHS,[†] we obtain

$$214 \quad \frac{Dq}{Dt} = \frac{D}{Dt} \left(\frac{\boldsymbol{\omega}_a}{\rho} \cdot \nabla\lambda \right) = \frac{\boldsymbol{\omega}_a}{\rho} \cdot \nabla\Psi + \nabla\lambda \cdot \frac{\nabla\rho \times \nabla p}{\rho^3} + \frac{\nabla\lambda}{\rho} \cdot \left(\nabla \times \frac{\mathcal{F}}{\rho} \right). \quad (2.9)$$

215 Choosing, for example, density (or a quantity proportional to density) as our scalar $\lambda = \rho$,
216 while requiring frictional and diabatic processes to be zero so that the flow is inviscid and
217 density is conserved, we see that all three terms on the RHS vanish and $q = (\boldsymbol{\omega}_a/\rho) \cdot \nabla\lambda$ is
218 conserved following fluid parcels. This is Ertel's PV theorem.

219

2.4. Absolute angular momentum

220

221 One of the contributions of Rayleigh (1917) was to demonstrate that, if a vortex is
222 axisymmetric (i.e. $\partial/\partial\phi = 0$), then the azimuthal momentum equation can be multiplied
223 by r and re-expressed as a conservation equation for the angular momentum per unit mass:
224 $D/Dt(r\bar{v}) = 0$, where \bar{v} denotes the azimuthal velocity. Application of this approach to a
225 fluid parcel in a rotating reference frame with constant rotation rate also permits such a
226 rearrangement: $DL/Dt = 0$, where $L = r\bar{v} + fr^2/2$ is now the *absolute angular momentum*,
227 and is the sum of relative angular momentum ($r\bar{v}$) and planetary angular momentum imparted
228 by the rotating reference frame. Importantly, the absolute angular momentum of a fluid parcel
229 in a vortex on the f -plane is *exactly the same as if the vortex were located at the center of*
230 *the rotating reference frame*, where r is the magnitude of the position vector (Kloosterziel &
231 van Heijst 1991). **This motivates the following vector representation.**

231

232 We orient our coordinate system so that its origin is at the center of a curved front or vortex
233 (cf. Figure 4). Taking the cross product of the position vector \mathbf{r}_c and each of the terms in
234 Equation 2.3, one obtains after some effort

$$234 \quad \frac{D\mathbf{m}_a}{Dt} = -\boldsymbol{\Omega}_o \times \mathbf{m} - \frac{\mathbf{r}_c \times \nabla p}{\rho} + \mathbf{r}_c \times \mathbf{g} + \frac{\mathbf{r}_c \times \mathcal{F}}{\rho}, \quad (2.10)$$

235

236 where $\mathbf{m}_a = \mathbf{r}_c \times \mathbf{u}_a$ and $\mathbf{m} = \mathbf{r}_c \times \mathbf{u}$ are absolute and relative angular momentum,
237 respectively. Using the definition of absolute velocity, $\mathbf{u}_a = \mathbf{u} + \boldsymbol{\Omega}_o \times \mathbf{r}_c$, we observe that
238 $\mathbf{m}_a = \mathbf{m} + \mathbf{m}_\Omega$ is the sum of relative angular momentum $\mathbf{m} = \mathbf{r}_c \times \mathbf{u}$ and planetary angular
239 momentum $\mathbf{m}_\Omega = \mathbf{r}_c \times (\boldsymbol{\Omega}_o \times \mathbf{r}_c)$ in a manner analogous to absolute vorticity $\boldsymbol{\omega}_a$.

239

240 For our purposes, we wish to isolate the vertical component of absolute angular momentum.
241 We take the inner product of Equation 2.10 and the vertical unit vector $\hat{\mathbf{k}}$ to obtain

$$241 \quad \frac{DL}{Dt} = -(\boldsymbol{\Omega}_o \times \mathbf{m}) \cdot \hat{\mathbf{k}} - \frac{\mathbf{r}_c \times \nabla p}{\rho} \cdot \hat{\mathbf{k}} + (\mathbf{r}_c \times \mathbf{g}) \cdot \hat{\mathbf{k}} + \frac{\mathbf{r}_c \times \mathcal{F}}{\rho} \cdot \hat{\mathbf{k}}, \quad (2.11)$$

242

243 where we have introduced the notation $L = \mathbf{m}_a \cdot \hat{\mathbf{k}}$ to denote the vertical component of
244 absolute angular momentum, consistent with the literature (Holton 1992; Shakespeare 2016).

[†] This follows from $\mathbf{A} \cdot \frac{D(\nabla\lambda)}{Dt} = \mathbf{A} \cdot \nabla \frac{D\lambda}{Dt} - \nabla\lambda \cdot (\mathbf{A} \cdot \nabla\mathbf{u})$, where $\mathbf{A} = \boldsymbol{\omega}_a/\rho$.

244 Thus, the vertical component of absolute angular momentum L of a fluid parcel is modified
 245 by torques due to pressure, gravitation, and friction, as well as a torque produced by Earth's
 246 rotation acting on the relative angular momentum \mathbf{m} . For cases when \mathbf{m} is not vertical, the
 247 latter reduces L , tilting the absolute angular momentum vector away from the vertical.

248 *A comparison with angular momentum conservation on the spheroid*

249 It is helpful to compare the conservation equation above (cf. Equation 2.10) with that obtained
 250 for the oblate sphere (e.g. Barnes *et al.* 1983; Peixoto & Oort 1992; Bell 1994). In spherical
 251 coordinates, the position vector \mathbf{r} extends from Earth's center to the fluid parcel (Figure 3).
 252 Computing the cross product of \mathbf{r} and the more general equations of motion (cf. Equation 2.1)
 253 gives (e.g. Egger 2001, Equation 2.7)

$$254 \quad \frac{D\mathbf{m}_a}{Dt} = -\boldsymbol{\Omega} \times \mathbf{m}_a - \frac{\mathbf{r} \times \nabla p}{\rho} + \mathbf{r} \times \underbrace{(\mathbf{g} - \mathbf{a}_c)}_{\mathbf{g}^*} + \frac{\mathbf{r} \times \mathcal{F}}{\rho}, \quad (2.12)$$

255 where absolute, relative, and planetary angular momentum are now given by $\mathbf{m}_a = \mathbf{m} + \mathbf{m}_\Omega$,
 256 $\mathbf{m} = \mathbf{r} \times \mathbf{u}$, and $\mathbf{m}_\Omega = \mathbf{r} \times (\boldsymbol{\Omega} \times \mathbf{r})$, respectively. A useful simplification can now be made.
 257 Expanding the first term on the RHS and examining only the planetary portion, we see that
 258 Earth's rotation induces a torque with magnitude $|\boldsymbol{\Omega} \times \mathbf{m}_\Omega| = |\mathbf{r}_\parallel| |\boldsymbol{\Omega}| |\boldsymbol{\Omega} \times \mathbf{r}_\perp| = |\boldsymbol{\Omega}|^2 |\mathbf{r}_\perp| |\mathbf{r}_\parallel|$
 259 and directed eastward.† Similarly, the torque induced by the centrifugal acceleration has
 260 magnitude $|\mathbf{r} \times \mathbf{a}_c| = |\boldsymbol{\Omega}|^2 |\mathbf{r}_\perp| |\mathbf{r}_\parallel|$ and is directed westward. The two terms cancel and
 261 Equation 2.12 becomes

$$262 \quad \frac{D\mathbf{m}_a}{Dt} = -\boldsymbol{\Omega} \times \mathbf{m} - \frac{\mathbf{r} \times \nabla p}{\rho} + \mathbf{r} \times \mathbf{g} + \frac{\mathbf{r} \times \mathcal{F}}{\rho}. \quad (2.13)$$

263 Therefore, Equation 2.10 is identical to Equation 2.13 is except where \mathbf{r} is replaced by \mathbf{r}_c
 264 and $\boldsymbol{\Omega}$ by $\boldsymbol{\Omega}_o$. This fact follows from the self-consistency of the governing equations on the f
 265 plane (Grimshaw 1975). Thus, while a formal proof remains, we argue that absolute angular
 266 momentum is conserved on the f plane in the same way that it is conserved on the sphere.‡
 267 This may be why, for sufficiently small horizontal scales and balanced (*i.e.* hydrostatic) flows
 268 in which the meridional component of Coriolis is neglected, the volume-integrated, vertical
 269 component of absolute angular momentum is approximately conserved (Egger 2001, Fig. 2e).

270 2.5. A vorticity theorem for the f plane

271 We are now in a position to combine conservation laws (cf. Equations 2.9 and 2.11). It is
 272 simple to show that if $\frac{DA}{Dt} = 0$ and if $\frac{DB}{Dt} = 0$, then $\frac{D}{Dt}(AB) = 0$. This is the logic behind the
 273 following step. We therefore multiply Equation 2.9 by $L = \mathbf{m}_a \cdot \hat{\mathbf{k}} = (\mathbf{m} + \mathbf{m}_\Omega) \cdot \hat{\mathbf{k}}$ and add
 274 this to $q = (\boldsymbol{\omega}_a/\rho) \cdot \nabla \lambda$ multiplied by Equation 2.11. This gives

$$275 \quad \frac{D}{Dt}(Lq) = L \left[\frac{\boldsymbol{\omega}_a}{\rho} \cdot \nabla \Psi + \nabla \lambda \cdot \frac{\nabla \rho \times \nabla p}{\rho^3} + \frac{\nabla \lambda}{\rho} \cdot \left(\nabla \times \frac{\mathcal{F}}{\rho} \right) \right]
 276 \quad + q \left[-(\boldsymbol{\Omega}_o \times \mathbf{m}) \cdot \hat{\mathbf{k}} - \frac{\mathbf{r}_c \times \nabla p}{\rho} \cdot \hat{\mathbf{k}} + (\mathbf{r}_c \times \mathbf{g}) \cdot \hat{\mathbf{k}} + \frac{\mathbf{r}_c \times \mathcal{F}}{\rho} \cdot \hat{\mathbf{k}} \right], \quad (2.14)$$

† Note: $\boldsymbol{\Omega} \times \mathbf{r} = \boldsymbol{\Omega} \times \mathbf{r}_\perp$ together with $\mathbf{A} \times (\mathbf{B} \times \mathbf{C}) = (\mathbf{A} \cdot \mathbf{C})\mathbf{B} - (\mathbf{A} \cdot \mathbf{B})\mathbf{C}$ allow us to write the planetary angular momentum as $\mathbf{m}_\Omega = |\mathbf{r}_\perp|^2 \boldsymbol{\Omega} - |\mathbf{r}_\parallel| |\boldsymbol{\Omega}| \mathbf{r}_\perp$.

‡ Egger (2001) did not demonstrate this vector cancellation and led him to conclude that angular momentum conservation was different in the f plane approximation than on the spheroid (in the limit of small aspect ratio $\delta = |ds|/R_e$). We disagree with this statement for the reasons stated above, although we acknowledge Egger (2001) was principally concerned with the β plane approximation.

10

277 where we emphasize that \mathbf{r}_c is the position vector in the cylindrical coordinate system and \mathbf{g}
 278 is directed anti-parallel to the unit vector $\hat{\mathbf{k}}$ (Figure 4).

279 Equation 2.14 states that the scalar Lq is conserved following fluid parcels on the f plane
 280 if, for non-zero L and q , all of the following conditions are met:

281 (i) density is conserved ($\Psi = 0$)

282 (ii) the fluid is inviscid ($\mathcal{F} = 0$)

283 (iii) the fluid is barotropic ($\nabla\rho \times \nabla p = 0$) **or** the fluid is baroclinic ($\nabla\rho \times \nabla p \neq 0$) and λ
 284 is chosen to be a “thermodynamic variable”

285 (iv) relative angular momentum \mathbf{m} is directed vertically so that $(\boldsymbol{\Omega}_o \times \mathbf{m}) \cdot \hat{\mathbf{k}} = 0$

286 (v) pressure torques are zero or orthogonal to the vertical so that $(\mathbf{r}_c \times \nabla p) \cdot \hat{\mathbf{k}} = 0$

287 (vi) perturbations in Earth’s gravitational field are zero so that $(\mathbf{r}_c \times \mathbf{g}) \cdot \hat{\mathbf{k}} = 0$, and

288 While this equation may find reduced application when compared to Ertel’s PV theorem,
 289 several simplifications are possible. For inviscid, adiabatic baroclinic flows, selecting λ as
 290 proportional to density (*e.g.* $\lambda = -\rho g$) satisfies conditions (i)-(iii). For geophysical flows of
 291 the type considered here, the flow is nearly two-dimensional such that \mathbf{m} points approximately
 292 vertically and condition (iv) is met. For azimuthally symmetric flow away from boundaries
 293 pressure gradient torques are zero, so that (v) is satisfied. (Undulating bottom topography will
 294 introduce pressure torques.) Finally, in the absence of geopotential perturbations, the sixth
 295 term is zero. In conclusion, we have a vorticity theorem valid on the f plane but different
 296 than Ertel’s PV theorem and yet, at least in highly curved flows away from boundaries, has
 297 the potential to satisfy all of the aforementioned conditions. *If these conditions are met,*
 298 *the product of the vertical component of absolute angular momentum and Ertel PV (Lq) is*
 299 *conserved following fluid parcels.*

300 3. Discussion

301 It is not clear how best to refer to the quantity Lq . We were at first tempted to refer to
 302 this quantity as the generalized potential vorticity since fluid parcels have possible vorticity
 303 values set by the sign of Lq through the stability discriminant $\Phi = 2Lq/r^2$ (Buckingham *et al.*
 304 2020*a,b*). However, the validity of the theorem is restricted to small horizontal scales such
 305 that Lq is not universally conserved. For this reason, *submesoscale potential vorticity* is a
 306 suitable alternative. † However, to avoid conflict with the Ertel PV and given its relationship
 307 to angular momentum (Rayleigh 1917; Solberg 1936; Fjortoft 1950), we adopt the term
 308 *potential momentum* below (denoting it as $\Pi = Lq$), in order to reflect that changes in
 309 angular momentum (or curvature) can occur as a result of alterations in the baroclinic nature
 310 of the fluid.

311 Given the restriction to the f plane and our interest in the oceans, the conservation theorem
 312 will find greatest application in understanding vortex flows at mid-to-high-latitudes in the
 313 oceanic submesoscale regime. Here, we have in mind curved fronts and vortices found at
 314 hydrothermal vents and convective plumes (Helfrich & Battisti 1991; D’Asaro *et al.* 1994;
 315 Legg & McWilliams 2001; Deremble 2016), within mid-latitude vortices (McDowell &
 316 Rossby 1978; McWilliams 1985; Riser *et al.* 1986; Bane *et al.* 1989; Konstantinoy & Belkin
 317 1989; Lilly & Rhines 2002; Bosse *et al.* 2016; Meunier *et al.* 2018), and polar mesoscale
 318 vortices (D’Asaro 1988; Timmermans *et al.* 2008; Zhao *et al.* 2014). The theorem may also
 319 aid in better understanding laboratory vortex flows (Stegner *et al.* 2004; Kloosterziel *et al.*
 320 2007; Lazar *et al.* 2013) and parcel motion within highly curved fronts in the upper ocean

† The scalar $\Phi/f = 2Lq/(fr^2) = (1 + \text{Cu})q$ is perhaps a better variable to be named “submesoscale potential vorticity” since it shares the same units as q and applies to straight and curved fronts. One recovers the Ertel PV in the limit $\text{Cu} \rightarrow 0$.

321 (M. Freilich 2020, personal communication). Such examples are frequently found in strong
322 boundary currents (*e.g.* Gulf Stream and Kuroshio) and the Southern Ocean.

323 While presenting a framework for understanding sources and sinks of “potential mo-
324 mentum” (Haynes & McIntyre 1987, 1990; Marshall & Nurser 1992) is beyond the scope
325 of this study, one can nevertheless conceptually consider the theorem’s application to the
326 aforementioned flows by expressing Equation 2.14 for an axisymmetric vortex flow. This is
327 done below, followed by a discussion of the conservation principle’s imprint on vorticity.

328 3.1. Axisymmetric vortex flow

329 We consider an axisymmetric vortex flow set at high latitudes in cyclogeostrophic and hy-
330 drostatic balance (*i.e.* GWB). We assume the flow is located in shallow waters ($|z| < 100$ m).
331 Examples can be found in the halocline eddies observed in the Arctic (Timmermans *et al.*
332 2008) but we could equally consider application to highly curved fronts in this region
333 (MacKinnon *et al.* 2021). Frictional and diabatic effects are weak such that this balance holds
334 (Eliassen 1951). Formally, we state that deviations from the balanced state are small such
335 that $\mathbf{u} = \bar{\mathbf{u}} + \mathbf{u}^* \approx (0, \bar{v}, 0)$ and $b = \bar{b} + b^* \approx \bar{b}$, where the overbar denotes mean quantities
336 and asterisks (*) denote perturbations from this state. We neglect compressibility, make the
337 Boussinesq approximation, and define $\lambda = -g\rho$, allowing the Ertel PV to be written as
338 $q = \omega_a \cdot \nabla b$, where $b = -g\rho/\rho_o$ is buoyancy and ρ_o is a constant reference density. Finally,
339 we set the meridional component of Coriolis to zero given its distance from the Equator.

340 We now express Equation 2.14 in cylindrical coordinates. The vertical component
341 of absolute angular momentum is $L = \mathbf{m}_a \cdot \hat{\mathbf{k}} = (\mathbf{m} + \mathbf{m}_\Omega) \cdot \hat{\mathbf{k}}$, where $\mathbf{m} = \mathbf{r}_c \times \mathbf{u}$ and
342 $\mathbf{m}_\Omega = \mathbf{r}_c \times (\Omega \times \mathbf{r}_c)$ are the relative and planetary angular momentum. Together with
343 $\mathbf{r}_c = (r, \phi, z)$, $\mathbf{u} = (u, v, w)$, and $\Omega = (0, 0, f)$, we find $L = r\bar{v} + fr^2/2$. The Ertel PV for
344 this vortex is $q = (2\Omega + \nabla \times \mathbf{u}) \cdot \nabla b$. Together with GWB $(f + 2\bar{v}/r)\partial_z \bar{v} = \partial_r \bar{b} = M^2$, we
345 have $q = (f + \bar{\zeta})N^2 - (f + 2\bar{v}/r)|\partial_z \bar{v}|^2$, where we have neglected the horizontal vorticity
346 owing to its smallness relative to other terms. The relative vorticity associated with the
347 balanced state is $\bar{\zeta} = (1/r)\partial_r(r\bar{v}) = \bar{v}/r + \partial_r \bar{v}$ and vertical stratification is $N^2 = \partial_z \bar{b}$. With
348 these definitions in hand, Equation 2.14 becomes

$$349 \quad \frac{D\Pi}{Dt} = S_{\mathcal{F}+\mathcal{D}+\mathcal{P}+q+\Omega}, \quad (3.1)$$

350 where the potential momentum is

$$351 \quad \Pi = Lq = \left(r\bar{v} + \frac{fr^2}{2} \right) \left[(f + \bar{\zeta})N^2 - \left(f + \frac{2\bar{v}}{r} \right) |\partial_z \bar{v}|^2 \right] = \frac{r^2\Phi}{2} \quad (3.2)$$

352 and $S_{\mathcal{F}+\mathcal{D}+\mathcal{P}+q+\Omega}$ represents sources and sinks of momentum due to frictional, diabatic,
353 pressure, and gravitational sources, as well as Earth’s rotation acting on the relative
354 momentum (*i.e.* RHS of Equation 2.14). Note: Φ is the generalized Rayleigh discriminant
355 and consists of barotropic and baroclinic components (Yim *et al.* 2019; Buckingham *et al.*
356 2020a):

$$357 \quad \Phi = (f + 2\bar{v}/r)(f + \bar{\zeta})N^2 - (f + 2\bar{v}/r)^2 |\partial_z \bar{v}|^2 = \underbrace{\chi^2 N^2}_{\text{barotropic}} - \underbrace{M^4}_{\text{baroclinic}}, \quad (3.3)$$

358 where $\chi^2 = (f + 2\bar{v}/r)(f + \bar{\zeta})$ is the generalized Rayleigh discriminant for barotropic
359 vortices (Kloosterziel & van Heijst 1991; Mutabazi *et al.* 1992). We can define non-
360 dimensional gradient Rossby, gradient Richardson, and curvature numbers as $Ro = \bar{\zeta}/f$,

12

361 $Ri = N^2/|\partial_z \bar{v}|^2$, and $Cu = 2\bar{v}/fr$, allowing us to also write the potential momentum as

$$362 \quad \Pi = Lq = \left(\frac{f^2 N^2 r^2}{2} \right) \Phi', \quad (3.4)$$

363 where

$$364 \quad \Phi' = L'q' = (1 + Cu)(1 + Ro) - (1 + Cu)^2 \cdot Ri^{-1}. \quad (3.5)$$

365 is a nondimensional form of the Rayleigh discriminant, and $L' = 1 + Cu$ and q' denote
366 nondimensional forms of L and q , respectively. Expanding Equation 3.1, we find

$$367 \quad \frac{D\Phi}{Dt} = 2S_{\mathcal{F}+\mathcal{D}+\mathcal{P}+q+\Omega} - \frac{2u}{r}\Phi. \quad (3.6)$$

368 In the absence of sources and sinks of potential momentum ($S_{\mathcal{F}+\mathcal{D}+\mathcal{P}+q+\Omega} = 0$) and assuming
369 no cross-frontal motion ($u = 0$), the stability of the flow is constant: $D\Phi/Dt = 0$. However,
370 if a fluid parcel moves radially ($u \neq 0$)—even in the absence of sources and sinks of potential
371 momentum—there must be a corresponding change in the stability of the flow.

372 We now make a clarifying comment. It was previously suggested that the theorem may find
373 utility in understanding parcel motion at curved baroclinic fronts. As a fluid parcel is advected
374 along its path in a meandering flow, we generally expect cross-frontal motion (Bower 1989;
375 Samelson 1992). However, as evidenced by Equation 3.6, Φ is not conserved. Moreover,
376 $D\Phi/Dt = 0$ does not imply $D\Phi'/Dt = 0$, except if N^2 and r^2 do not change following a
377 fluid parcel (cf. Equation 3.4). These conditions can be met within the axisymmetric vortex
378 ($\partial_\phi \bar{b} \approx 0$ and $u \approx 0$) but will not generally be met following fluid parcels within a meandering
379 front. These points therefore clarify statements made by Buckingham *et al.* (2020a,b).

380 3.1.1. A special case: $S_{\mathcal{F}+\mathcal{D}+\mathcal{P}+q+\Omega} = 0$

381 One of the consequences of Equation 2.14 is that geophysical vortices which reside away from
382 boundaries and perturbations in Earth's geopotential approximately conserve the product of
383 L and q . In the absence of sources and sinks of potential momentum ($S_{\mathcal{F}+\mathcal{D}+\mathcal{P}+q+\Omega} = 0$), we
384 can safely approximate cross-frontal motion within an axisymmetric vortex as zero ($u \approx 0$).
385 By virtue of Equation 3.6, this also implies that the Rayleigh discriminant Φ is conserved:
386 $D\Phi/Dt \approx 0$. To understand the consequences of these statements, we consider the evolution
387 of small-scale baroclinic vortices discussed by Buckingham *et al.* (2020b).

388 While the details of this evolution remain unclear without corroborating model support,
389 the following arguments are reasonable. Small-scale baroclinic vortices (radii of 1–10 km)
390 are typically generated in proximity to ocean boundaries due to horizontal shear, baroclinic
391 instability, and convection (Barkley 1972; Legg & McWilliams 2001; Eldevik & Dysthe
392 2002; Boccaletti *et al.* 2007; Stegner 2014; Bosse *et al.* 2016; Gula *et al.* 2016; MacKinnon
393 *et al.* 2019; Srinivasan *et al.* 2019; Wenegrat *et al.* 2018). These boundaries include the ocean
394 surface, bottom boundary, and ice-ocean boundary. Immediately following formation, they
395 undergo a form of cyclogeostrophic adjustment (Stegner *et al.* 2004), trapping and carrying
396 with them water properties reflective of the boundary layers in which they were formed.

397 Boundary layer fluid is often characterized by reduced stratification such that, in the
398 presence of vertical shears, $Ri \sim 1$. If this fluid is trapped within the vortex core, then the
399 fluid with low Ri will persist even as the vortex subducts or is advected away from the
400 boundary. One measure of this trapping is the metric \bar{v}/c , where \bar{v} is the azimuthal velocity
401 and c is the translation speed of the vortex (Samelson 1992). It follows that the results from
402 Buckingham *et al.* (2020b) apply. That is, symmetric instability will be active within cyclonic
403 vortices, while anticyclonic vortices will remain marginally stable, decaying over longer time

404 scales due to weak inertial-symmetric instabilities.† If the vortex is advected into a different
 405 environment, the vortex must alter barotropic and baroclinic components of Φ so as to keep
 406 Φ constant. Thus, stratification, shear, and centripetal accelerations (cf. Equation 3.3) must
 407 change. In non-dimensional form (cf. Equations 3.4 and 3.5), we see that Ro , Ri , and Cu must
 408 change in concert so as to conserve $\Pi = Lq$. Note: Equation 3.4 applies but $D/Dt(N^2) \neq 0$.

409 3.2. Revisiting the distribution of relative vorticity

410 We return to the joint PDF of vorticity and strain rate observed near the Gulf Stream
 411 (Figure 1). We previously noted that as vorticity increased in the cyclonic direction, the
 412 joint PDF approached a pure shear relationship, indicative of straight fronts. In contrast,
 413 the vorticity was bounded as vorticity decreased toward the negative direction, and a higher
 414 probability of vortex flow. While the unbounded nature of cyclonic vorticity associated
 415 with straight fronts can be rationalized in terms of PV conservation (Hoskins & Bretherton
 416 1972)‡, the higher probability of anticyclonic vorticity associated with vortex flow has not
 417 been explained.

418 Requiring $Lq > 0$ for all time requires $\Phi > 0$ for all time since $Lq = r^2\Phi/2$. In this case,
 419 $D/Dt(Lq) = 0$ together with an initial positive state $Lq > 0$ places constraints on the sign
 420 of Φ and determines the distribution of relative vorticity in the oceans. This is analogous to
 421 how $Dq/Dt = 0$ together with an initial positive state $fq > 0$ determines the distribution of
 422 relative vorticity at straight fronts (Buckingham *et al.* 2016). Another way to state this is that
 423 the statistics of vorticity are determined by the possible set of Rossby numbers which ensure
 424 the stability discriminant is positive: $\Phi > 0$ or $\Phi' > 0$. If one requires that Equation 3.3 or 3.5
 425 be positive and solves for the set of Rossby numbers which ensure this is true, the negative
 426 skewness discussed above will emerge at low Ri (Buckingham *et al.* 2020b).

427 Figure 5 displays $\Phi' = L'q'$ (cf. Equation 3.5) for a range of Richardson, Rossby, and
 428 curvature numbers characteristic of a Gaussian vortex in the upper ocean. For clarity, we
 429 identify regions of centrifugal and symmetric instability. While Φ' is locally evaluated (here,
 430 at the radius of maximum velocity r_m) and cannot describe the global stability of a vortex
 431 flow, this nonetheless demonstrates an important point: centripetal accelerations or curvature
 432 can shape the distribution of Ro . In particular, for $Ri = 1.0$, anticyclonic flow is (weakly)
 433 stable while cyclonic flow is significantly unstable. We therefore expect to see a greater
 434 occurrence of anticyclonic vortex flow at $Ri \sim 1$. This is remarkably different than if the
 435 front were geostrophic, which predicts cyclonic flow: $Ro > -1 + Ri^{-1}$, or $Ro > 0$.

436 We now demonstrate this analytically. Introducing a non-dimensional parameter
 437 $\mu = Cu/Ro$, which is independent of depth and positive definite within the vortex
 438 core ($0 < r < r_m$), and examining solutions for $Ri < \mu$ subject to $\Phi' > 0$, one finds
 439 that vorticity Ro principally resides between two curves in dimensionless space, or
 440 marginal stability curves (Buckingham *et al.* 2020b): $Ro_0 = -\mu^{-1}$ (barotropic root) and
 441 $Ro_1 = -(Ri - 1)/(Ri - \mu)$ (baroclinic root). The barotropic root corresponds to the threshold
 442 for centrifugal instability ($Cu = -1$), while the baroclinic root corresponds to the threshold
 443 for symmetric instability. Selecting $Ri = 1$, one finds that gradient Rossby numbers lie
 444 between $-\mu^{-1}$ and 0. Arbitrarily choosing $\mu = 2.0$ (characteristic of Gaussian vortices at

† A timescale for the decay of the cyclonic vortex can be estimated from the growth rate of symmetric disturbances: $T = 2\pi/\sigma$, where $\sigma = f(-\Phi')^{1/2}$ is an approximate growth rate of symmetric disturbances under a simplified axisymmetric vortex model (Buckingham *et al.* 2020a, Appendix A). Mahdinia *et al.* (2017) document a decay timescale greater than 50 eddy “turnaround times” for the anticyclonic vortex.

‡ Assuming an initially positive state $fq > 0$, $Dq/Dt = 0$ requires that fq remain positive for all future states. For geostrophic flow and positive stratification, $fq > 0$ can also be written in terms of gradient Rossby and Richardson numbers: $1 + Ro - Ri^{-1} > 0$. Since $Ri > 0$, it follows that Ro is unbounded in the cyclonic direction: $Ro > -1 + Ri^{-1}$.

14

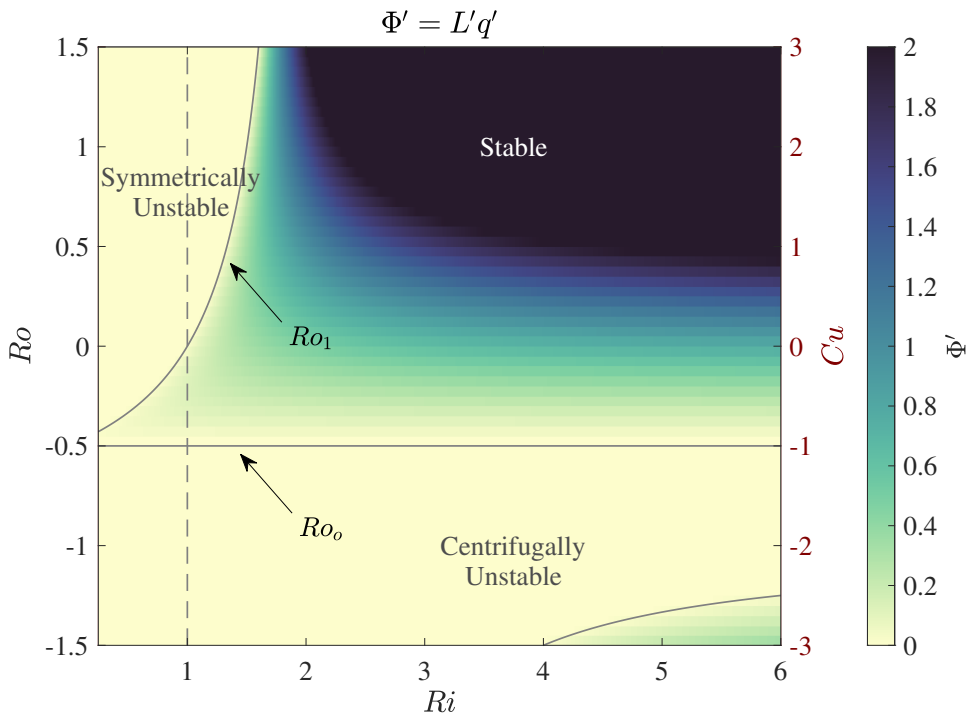


Figure 5: Stability discriminant $\Phi' = L'q'$ as a function of Ro , Ri , and Cu . Observed flows in which Lq is conserved are expected to reside within the stable region $\Phi' > 0$ (blue). This region is delineated from the unstable region (white) by the roots Ro_0 and Ro_1 of Φ' when expressed in terms of the ratio μ (see text). These roots correspond to thresholds for centrifugal and symmetric instability, respectively. For $Ri = 1$ (vertical dashed line), we observe only (weakly) stable anticyclonic flow. This is remarkably different than if the front were geostrophic, which predicts only cyclonic flow (not shown). The stable region in the bottom right corner corresponds to intense, stratified anticyclones for which $\Phi' > 0$, despite that L' and q' are both negative. Such a situation might occur as a result of flow past topography. This graphic is characteristic of Gaussian vortices at the radius of maximum velocity $r = r_m$ (*i.e.* valid for $\mu = 2$).

445 $r = r_m$) gives $-0.5 < Ro < 0$. That is, the vorticity must be anticyclonic if Lq is conserved.
 446 Mahdinia *et al.* (2017) find similar constraints on anticyclonic vortices in their numerical
 447 investigation of the stability of three-dimensional Gaussian vortices.

448 4. Limitations

449 Our derivation makes the f plane approximation and therefore is restricted to small horizontal
 450 scales. Additionally, we isolated the vertical component of absolute angular momentum. As
 451 a result, Equation 2.14 cannot be used predict Lq except at the poles since L is coupled to
 452 the other components of \mathbf{m}_a through $\mathbf{\Omega} \times \mathbf{m}$. As stated above, this term arises from Earth's
 453 rotation and tilts the absolute angular momentum vector away from the vertical, reducing L .
 454 This torque is greatest at the Equator and zero at the poles. This does not make Equation 2.14
 455 incorrect but simply limits its utility in certain cases. In summary, the two main limitations to
 456 the theory are (i) restriction to the f plane and (ii) reduced applicability in the tropics. These
 457 are important limitations since intense frontal flows are frequently found near the Equator
 458 (Marchesiello *et al.* 2011; Holmes *et al.* 2013; Simoes-Sousa *et al.* 2021). Progress in this
 459 area might be made by examining the recent work of Kloosterziel *et al.* (2017).

460 It may be worth noting that the f plane approximation together with angular momentum
 461 conservation principles have previously been successful for investigating tropical cyclone
 462 dynamics (Houze 1993), indicating that these limitations—which grow for vortices closer to
 463 the Equator—may not be so severe. It is probable that a more elegant intersection of these
 464 three principles will be presented in the future (*i.e.* Figure 2 but where L is replaced by m_a).

465 5. Conclusions

466 In this study, we have presented a vorticity equation valid on the f plane. It is an extension
 467 of Ertel's PV theorem to vortex flow at small horizontal scales such that absolute angular
 468 momentum can properly be defined. This leads to a non-trivial result: the combination of
 469 absolute angular momentum conservation together with Ertel's theorem has implications
 470 for the motion of fluid parcels. In particular, two important consequences of the theorem
 471 are (1) stratification, shear, and centripetal accelerations are modified in concert in an effort
 472 to conserve Lq and (2) modification to the distribution of relative vorticity opposite to
 473 that predicted by geostrophic theory, permitting the occurrence of stable anticyclonic flow,
 474 while limiting the occurrences of cyclonic flow at low Richardson numbers. That is, if
 475 $Lq > 0$ initially, then $D/Dt(Lq) = 0$ has important consequences for the range of vorticity
 476 values seen at small horizontal scales in the ocean. While this may find obvious application in
 477 explaining why submesoscale vortices are overwhelmingly anticyclonic, the theorem will also
 478 find use in understanding Lagrangian motion within highly curved baroclinic fronts. Given
 479 that our present theory of submesoscale flows assumes the mean state to be in geostrophic
 480 balance (Thomas *et al.* 2008; McWilliams 2016), the inclusion of centripetal accelerations
 481 at the submesoscale represents a shift in direction for the oceanographic community.

482 The topic of absolute angular momentum conservation has received little attention
 483 in oceanography texts, while this same topic has received considerable attention in the
 484 atmospheric literature (Holton 1992; Peixoto & Oort 1992; Barnes *et al.* 1983; Bell 1994).
 485 This appears to be due to the presence of continental boundaries in the ocean but which are
 486 absent in the atmosphere (Griffies 2004), causing PV rather than absolute angular momentum
 487 to be a more universally conserved quantity at large horizontal scales (Pedlosky 1987).
 488 An exception may be in the Southern Ocean, where obstacles to zonal flow are absent
 489 (Straub 1993). However, for small-scale geophysical flows in which centripetal accelerations
 490 are present and Earth's rotation plays a dynamically important role,† the conservation of
 491 absolute angular momentum finds its place. Submesoscale and polar mesoscale flows are
 492 ideal examples in which such a conservation principle may apply. It is in the context of these
 493 phenomena that the combined theorem should find greater use.

494 **Acknowledgements.** This study was initially made possible by an Individual Fellowship from the European
 495 Commission on centrifugal instability (2019-2020). The derivation was made in a two-month period
 496 following the fellowship. The author would like to acknowledge the following individuals for helpful
 497 conversations (in chronological order): George Nurser, Guillaume Roulet, Keith Nicholls, Greace Crystle,
 498 Charly DeMarez, Thomas Meunier, Stephen Griffies, Bruno Deremble, and Amit Tandon.

499 **Declaration of interests.** The authors report no conflict of interest.

500 **Data availability statement.** No data were used in this study.

† Earth's rotation imparts angular momentum to fluid parcels and can limit centripetal accelerations present in anticyclonic flow through the constraint, $L' = 1 + Cu > 0$, assuming $Cu > -1$ initially. This is analogous to how Earth's rotation imparts vorticity to fluid parcels and limits horizontal shear present in anticyclonic barotropic flow through the constraint, $1 + Ro > 0$.

REFERENCES

- 501 ADAMS, KATHERINE A., HOSEGOOD, PHILIP, TAYLOR, JOHN R., SALLÉE, JEAN-BAPTISTE, BACHMAN, SCOTT,
502 TORRES, RICARDO & STAMPER, MEGAN 2017 Frontal circulation and submesoscale variability during
503 the formation of a Southern Ocean mesoscale eddy. *Journal of Physical Oceanography* **47** (7),
504 1737–1753.
- 505 BANE, J. M., O'KEEFE, L. M., WATTS, D. R., NIHOUL, J. C. J. & JAMART, B. M. 1989 *Mesoscale Eddies*
506 *and Submesoscale, Coherent Vortices: Their Existence Near and Interactions with the Gulf Stream,*
507 *Elsevier Oceanography Series*, vol. 50, pp. 501–518. Elsevier.
- 508 BARKLEY, RICHARD A. 1972 Johnston Atoll's wake. *Journal of Marine Research* **30** (2), 201–216.
- 509 BARNES, R. T. H., HIDE, RAYMOND, WHITE, A. A. & WILSON, C. A. 1983 Atmospheric angular momentum
510 fluctuations, length-of-day changes and polar motion. *Proceedings of the Royal Society of London.*
511 *A. Mathematical and Physical Sciences* **387** (1792), 31–73.
- 512 BATCHELOR, G. K. 1967 *An Introduction to Fluid Dynamics*. Cambridge: Cambridge University Press.
- 513 BELL, M. J. 1994 Oscillations in the equatorial components of the atmosphere's angular momentum and
514 torques on the Earth's bulge. *Quarterly Journal of the Royal Meteorological Society* **120** (515),
515 195–213.
- 516 BOCCALETTI, GIULIO, FERRARI, RAFFAELE & FOX-KEMPER, BAYLOR 2007 Mixed layer instabilities and
517 restratification. *Journal of Physical Oceanography* **37** (9), 2228–2250.
- 518 BOSSE, ANTHONY, TESTOR, PIERRE, HOUPERT, LOIC, DAMIEN, PIERRE, PRIEUR, LOUIS, HAYES, DANIEL,
519 TAILLANDIER, VINCENT, DURRIEU DE MADRON, XAVIER, D'ORTENZIO, FABRIZIO, COPPOLA,
520 LAURENT, KARSTENSEN, JOHANNES & MORTIER, LAURENT 2016 Scales and dynamics of
521 submesoscale coherent vortices formed by deep convection in the northwestern Mediterranean Sea.
522 *Journal of Geophysical Research: Oceans* **121** (10), 7716–7742.
- 523 BOWER, AMY S. 1989 Potential vorticity balances and horizontal divergence along particle trajectories in
524 Gulf Stream meanders east of Cape Hatteras. *Journal of Physical Oceanography* **19** (11), 1669–1681.
- 525 BUCKINGHAM, CHRISTIAN E., GULA, JONATHAN & CARTON, XAVIER 2020a The role of curvature in
526 modifying frontal instabilities, part 1. *Journal of Physical Oceanography* .
- 527 BUCKINGHAM, CHRISTIAN E., GULA, JONATHAN & CARTON, XAVIER 2020b The role of curvature in
528 modifying frontal instabilities, part 2. *Journal of Physical Oceanography* .
- 529 BUCKINGHAM, CHRISTIAN E., NAVEIRA GARABATO, ALBERTO C., THOMPSON, ANDREW F., BRANNIGAN,
530 LIAM, LAZAR, AYAH, MARSHALL, DAVID P., GEORGE NURSER, A. J., DAMERELL, GILLIAN, HEYWOOD,
531 KAREN J. & BELCHER, STEPHEN E. 2016 Seasonality of submesoscale flows in the ocean surface
532 boundary layer. *Geophys. Res. Lett.* **43**, 2118–2126, 2016GL068009.
- 533 CHELTON, DUDLEY B., DESZOEKE, ROLAND A., SCHLAX, MICHAEL G., EL NAGGAR, KARIM & STWERTZ,
534 NICOLAS 1998 Geographical variability of the first baroclinic rossby radius of deformation. *Journal*
535 *of Physical Oceanography* **28** (3), 433–460.
- 536 CUSHMAN-ROISIN, BENOIT 1994 *Introduction to Geophysical Fluid Dynamics*. Englewood Cliffs, N.J.:
537 Prentice Hall.
- 538 D'ASARO, ERIC, LEE, CRAIG, RAINVILLE, LUC, HARCOURT, RAMSEY & THOMAS, LEIF 2011 Enhanced
539 turbulence and energy dissipation at ocean fronts. *Science* **332** (6027), 318–322.
- 540 D'ASARO, ERIC, WALKER, SHARON & BAKER, EDWARD 1994 Structure of two hydrothermal megaplumes.
541 *Journal of Geophysical Research: Oceans* **99** (C10), 20361–20373.
- 542 D'ASARO, ERIC A. 1988 Observations of small eddies in the Beaufort Sea. *Journal of Geophysical Research:*
543 *Oceans* **93** (C6), 6669–6684.
- 544 DEREMBLE, BRUNO 2016 Convective plumes in rotating systems. *Journal of Fluid Mechanics* **799**, 27–55.
- 545 EGGER, JOSEPH 2001 Angular momentum of β -plane flows. *Journal of the Atmospheric Sciences* **58** (17),
546 2502–2508.
- 547 ELDEVIK, TOR & DYSTHE, KRISTIAN B. 2002 Spiral eddies. *Journal of Physical Oceanography* **32** (3),
548 851–869.
- 549 ELIASSEN, ARNT 1951 Slow thermally or frictionally controlled meridional circulation in a circular vortex.
550 *Astrophysica Norvegica* **5** (2), 1–42.
- 551 ERTEL, HANS 1942 Ein neuer hydrodynamischer wirbelsatz. *Meteorol. Z.* **59**, 271–281.
- 552 FJORTOFT, R. 1950 Application of integral theorems in deriving criteria of stability for laminar flows and
553 for the baroclinic circular vortex. *Geophys. Publ.* **17** (6), 1–52.
- 554 FLAMENT, PIERRE, ARMI, LAURENCE & WASHBURN, LIBE 1985 The evolving structure of an upwelling
555 filament. *Journal of Geophysical Research: Oceans* **90** (C6), 11765–11778.
- 556 GENTEMANN, C. L., SCOTT, JOEL P., MAZZINI, PIERO L. F., PIANCA, CASSIA, AKELLA, SANTHA, MINNETT,
Cambridge University Press

- 557 PETER J., CORNILLON, PETER, FOX-KEMPER, BAYLOR, CETINIĆ, IVONA, CHIN, T. MIKE, GOMEZ-
558 VALDES, JOSE, VAZQUEZ-CUERVO, JORGE, TSONTOS, VARDIS, YU, LISAN, JENKINS, RICHARD,
559 HALLEUX, SEBASTIEN DE, PEACOCK, DAVE & COHEN, NORA 2020 Saildrone: Adaptively sampling
560 the marine environment. *Bulletin of the American Meteorological Society* **101** (6), E744–E762.
- 561 GRIFFIES, STEPHEN M. 2004 *Fundamentals of Ocean Climate Models*. Princeton: Princeton University Press.
- 562 GRIMSHAW, R. H. J. 1975 A note on the β -plane approximation. *Tellus* **27** (4), 351–357.
- 563 GULA, JONATHAN, MOLEMAKER, M. JEROEN & MCWILLIAMS, JAMES C. 2016 Topographic generation of
564 submesoscale centrifugal instability and energy dissipation. *Nature Communications* **7**.
- 565 HAYNES, P. H. & MCINTYRE, M. E. 1987 On the evolution of vorticity and potential vorticity in the presence of
566 diabatic heating and frictional or other forces. *Journal of the Atmospheric Sciences* **44** (5), 828–841.
- 567 HAYNES, P. H. & MCINTYRE, M. E. 1990 On the conservation and impermeability theorems for potential
568 vorticity. *Journal of the Atmospheric Sciences* **47** (16), 2021–2031.
- 569 HELFRICH, KARL R. & BATTISTI, THOMAS M. 1991 Experiments on baroclinic vortex shedding from
570 hydrothermal plumes. *Journal of Geophysical Research: Oceans* **96** (C7), 12511–12518.
- 571 HOLMES, RYAN M., THOMAS, LEIF N., THOMPSON, LUANNE & DARR, DAVID 2013 Potential vorticity
572 dynamics of tropical instability vortices. *Journal of Physical Oceanography* **44** (3), 995–1011.
- 573 HOLTON, JAMES R. 1992 *An Introduction to Dynamic Meteorology*, 3rd edn. Academic Press.
- 574 HOSKINS, B. J. & BRETHERTON, F. P. 1972 Atmospheric frontogenesis models: mathematical formulation
575 and solution. *Journal of the Atmospheric Sciences* **29**, 11–37.
- 576 HOUZE, R. 1993 *Cloud dynamics, International Geophysics Series*, vol. 53. Academic Press.
- 577 KLOOSTERZIEL, R. C., CARNEVALE, G. F. & ORLANDI, P. 2007 Inertial instability in rotating and stratified
578 fluids: barotropic vortices. *Journal of Fluid Mechanics* **583**, 379–412.
- 579 KLOOSTERZIEL, R. C., CARNEVALE, G. F. & ORLANDI, P. 2017 Equatorial inertial instability with full Coriolis
580 force. *Journal of Fluid Mechanics* **825**, 69–108.
- 581 KLOOSTERZIEL, R. C. & VAN HEIJST, G. J. F. 1991 An experimental study of unstable barotropic vortices in
582 a rotating fluid. *Journal of Fluid Mechanics* **223**, 1–24.
- 583 KONSTIANOY, ANDREY G. & BELKIN, I. M. 1989 *A survey of observations on intrathermocline eddies in the*
584 *world ocean*, pp. 821–841. Elsevier Academic Press.
- 585 LAZAR, AYAH, STEGNER, A., CALDEIRA, R., DONG, C., DIDELLE, H. & VIBOUD, S. 2013 Inertial instability
586 of intense stratified anticyclones. part 2. laboratory experiments. *Journal of Fluid Mechanics* **732**,
587 485–509.
- 588 LEGG, SONYA & MCWILLIAMS, JAMES C. 2001 Convective modifications of a geostrophic eddy field. *Journal*
589 *of Physical Oceanography* **31** (4), 874–891.
- 590 LILLY, JONATHAN M. & RHINES, PETER B. 2002 Coherent eddies in the Labrador Sea observed from a
591 mooring. *Journal of Physical Oceanography* **32**, 585–598.
- 592 MACKINNON, JENNIFER A., ALFORD, MATTHEW H., VOET, GUNNAR, ZEIDEN, KRISTIN L.,
593 SHAUN JOHNSTON, T. M., SIEGELMAN, MIKA, MERRIFIELD, SOPHIA & MERRIFIELD, MARK 2019
594 Eddy wake generation from broadband currents near Palau. *Journal of Geophysical Research:*
595 *Oceans* **124** (7), 4891–4903.
- 596 MACKINNON, JENNIFER A., SIMMONS, HARPER L., HARGROVE, JOHN, THOMSON, JIM, PEACOCK, THOMAS,
597 ALFORD, MATTHEW H., BARTON, BENJAMIN I., BOURY, SAMUEL, BRENNER, SAMUEL D., COUTO,
598 NICOLE, DANIELSON, SETH L., FINE, ELIZABETH C., GRABER, HANS C., GUTHRIE, JOHN, HOPKINS,
599 JOANNE E., JAYNE, STEVEN R., JEON, CHANHYUNG, KLENZ, THILO, LEE, CRAIG M., LENN, YUENG-
600 DJERN, LUCAS, ANDREW J., LUND, BJÖRN, MAHAFFEY, CLAIRE, NORMAN, LOUISA, RAINVILLE, LUC,
601 SMITH, MADISON M., THOMAS, LEIF N., TORRES-VALDÉS, SINHUÉ & WOOD, KEVIN R. 2021 A warm
602 jet in a cold ocean. *Nature Communications* **12** (1), 2418.
- 603 MAHDINIA, MANI, HASSANZADEH, PEDRAM, MARCUS, PHILIP S. & JIANG, CHUNG-HSIANG 2017 Stability
604 of three-dimensional Gaussian vortices in an unbounded, rotating, vertically stratified, Boussinesq
605 flow: linear analysis. *Journal of Fluid Mechanics* **824**, 97–134.
- 606 MARCHESIELLO, PATRICK, CAPET, XAVIER, MENKES, CHRISTOPHE & KENNAN, SEAN C. 2011 Submesoscale
607 dynamics in tropical instability waves. *Ocean Modelling* **39** (1), 31–46.
- 608 MARSHALL, JOHN C. & NURSER, A. J. GEORGE 1992 Fluid dynamics of oceanic thermocline ventilation.
609 *Journal of Physical Oceanography* **22** (6), 583–595.
- 610 MCDOWELL, SCOTT E. & ROSSBY, H. THOMAS 1978 Mediterranean water: an intense mesoscale eddy off the
611 bahamas. *Science* **202**, 1085–1087.
- 612 MCWILLIAMS, JAMES C. 1985 Submesoscale, coherent vortices in the ocean. *Reviews of Geophysics* **23** (2),
613 165–182.

- 614 MCWILLIAMS, JAMES C. 2016 Submesoscale currents in the ocean. *Proceedings of the Royal Society of*
 615 *London A: Mathematical, Physical and Engineering Sciences* **472** (2189), 1–32.
- 616 MEUNIER, THOMAS, TENREIRO, M., PALLÀS-SANZ, ENRIC, OCHOA, JOSE, RUIZ-ANGULO, ANGEL, PORTELA,
 617 ESTHER, CUSÍ, SIMÓ, DAMIEN, PIERRE & CARTON, XAVIER 2018 Intrathermocline eddies embedded
 618 within an anticyclonic vortex ring. *Geophysical Research Letters* **45** (15), 7624–7633.
- 619 MÜLLER, PETER 1995 Ertel’s potential vorticity theorem in physical oceanography. *Reviews of Geophysics*
 620 **33** (1), 67–97.
- 621 MUNK, WALTER, ARMI, LAURENCE, FISCHER, KENNETH & ZACHARIASEN, F 2000 Spirals on the sea. In
 622 *Proceedings of the Royal Society of London A: Mathematical, Physical and Engineering Sciences*, ,
 623 vol. 456, pp. 1217–1280. The Royal Society.
- 624 MUTABAZI, INNOCENT, NORMAND, CHRISTIANE & WESFREID, JOSÉ EDUARDO 1992 Gap size effects on
 625 centrifugally and rotationally driven instabilities. *Physics of Fluids A: Fluid Dynamics* **4** (6), 1199–
 626 1205.
- 627 NAVEIRA GARABATO, ALBERTO C., FRAJKA-WILLIAMS, ELEANOR E., SPINGYS, CARL P., LEGG, SONYA,
 628 POLZIN, KURT L., FORRYAN, ALEXANDER, ABRAHAMSEN, E. POVL, BUCKINGHAM, CHRISTIAN E.,
 629 GRIFFIES, STEPHEN M., MCPHAIL, STEPHEN D., NICHOLLS, KEITH W., THOMAS, LEIF N. &
 630 MEREDITH, MICHAEL P. 2019 Rapid mixing and exchange of deep-ocean waters in an abyssal
 631 boundary current. *Proceedings of the National Academy of Sciences* **116** (27), 13233.
- 632 NURSER, A. J. GEORGE & BACON, SHELDON 2014 The Rossby radius in the Arctic Ocean. *Ocean Sci.* **10**,
 633 967–975.
- 634 ONKEN, R., BASCHEK, B. & ANGEL-BENAVIDES, I. M. 2020 Very high-resolution modelling of submesoscale
 635 turbulent patterns and processes in the Baltic Sea. *Ocean Science* **16** (3), 657–684.
- 636 PEDLOSKY, JOSEPH 1987 *Geophysical Fluid Dynamics*, 2nd edn. New York: Springer New York.
- 637 PEIXOTO, JOSE P. & OORT, ABRAHAM H. 1992 *Physics of Climate*, 1st edn. American Institute of Physics
 638 Press.
- 639 DU PLESSIS, MARCEL, SWART, SEBASTIAAN, ANSORGE, ISABELLE J., MAHADEVAN, AMALA & THOMPSON,
 640 ANDREW F. 2019 Southern Ocean seasonal restratification delayed by submesoscale wind–front
 641 interactions. *Journal of Physical Oceanography* **49** (4), 1035–1053.
- 642 RAYLEIGH, LORD 1917 On the dynamics of revolving fluids. *Proc. Royal Society of London. Series A,*
 643 *Containing Papers of a Mathematical and Physical Character* **93**, 148–154.
- 644 RILEY, K. F., HOBSON, M. P. & BENICE, S. J. 2006 *Mathematical Methods for Physics and Engineering: A*
 645 *Comprehensive Guide*, 3rd edn. Cambridge: Cambridge University Press.
- 646 RISER, STEPHEN C., OWENS, W. BRECHNER, ROSSBY, H. THOMAS & EBBESMEYER, CURTIS C. 1986 The
 647 structure, dynamics, and origin of a small-scale lens of water in the western North Atlantic
 648 thermocline. *Journal of Physical Oceanography* **16** (3), 572–590.
- 649 ROULLET, GUILLAUME & KLEIN, PATRICE 2010 Cyclone-anticyclone asymmetry in geophysical turbulence.
 650 *Physical Review Letters* **104** (21), 1–4.
- 651 RUDNICK, DANIEL L. 2001 On the skewness of vorticity in the upper ocean. *Geophysical Research Letters*
 652 **28** (10), 2045–2048.
- 653 SAMELSON, R. M. 1992 Fluid Exchange across a Meandering Jet. *Journal of Physical Oceanography* **22** (4),
 654 431–444.
- 655 SCULLY-POWER, PAUL 1986 Navy Oceanographer Shuttle observations, STS 41-G Mission Report. *Tech.*
 656 *Rep.*. DTIC Document, Newport, Rhode Island.
- 657 SHAKESPEARE, CALLUM J. 2016 Curved density fronts: Cyclogeostrophic adjustment and frontogenesis.
 658 *Journal of Physical Oceanography* **46**, 3193–3207.
- 659 SHCHERBINA, ANDREY Y., D’ASARO, ERIC A., LEE, CRAIG M., KLYMAK, JODY M., MOLEMAKER, M. JEROEN
 660 & MCWILLIAMS, JAMES C. 2013 Statistics of vertical vorticity, divergence, and strain in a developed
 661 submesoscale turbulence field. *Geophysical Research Letters* **40** (17), 4706–4711.
- 662 SIMOES-SOUSA, IURY T., SILVEIRA, ILSON CARLOS A., TANDON, AMIT, FLIERL, GLENN R., RIBEIRO, CESAR
 663 H. A. & MARTINS, RENATO P. 2021 The Barreirinhas eddies: Stable energetic anticyclones in the
 664 near-equatorial South Atlantic. *Frontiers in Marine Science* **8**, 28.
- 665 SMITH, K. SHAFER 2007 The geography of linear baroclinic instability in Earth’s oceans. *Journal of Marine*
 666 *Research* **65** (5), 655–683.
- 667 SOLBERG, H. 1936 Le mouvement d’inertie de l’atmosphère stable et son rôle dans la théorie des cyclones.
 668 In *Sixth Assembly*, pp. 66–82. Union Geodesique et Geophysique Internationale, Edinburgh: Paul
 669 Dupont.
- 670 SRINIVASAN, KAUSHIK, MCWILLIAMS, JAMES C., MOLEMAKER, M. JEROEN & BARKAN, ROY 2019

- 671 Submesoscale vortical wakes in the lee of topography. *Journal of Physical Oceanography* **49** (7),
672 1949–1971.
- 673 STEGNER, ALEXANDRE 2014 *Oceanic Island Wake Flows in the Laboratory*, chap. 14, pp. 265–276. American
674 Geophysical Union (AGU).
- 675 STEGNER, A., BOURET-AUBERTOT, P. & PICHON, T. 2004 Nonlinear adjustment of density fronts. Part 1. the
676 Rossby scenario and the experimental reality. *Journal of Fluid Mechanics* **502**, 335–360.
- 677 STRAUB, DAVID N. 1993 On the transport and angular momentum balance of channel models of the Antarctic
678 Circumpolar Current. *Journal of Physical Oceanography* **23** (4), 776–782.
- 679 THOMAS, LEIF N. & LEE, CRAIG M. 2005 Intensification of ocean fronts by down-front winds. *J. Phys.*
680 *Oceanogr.* **35**, 1086–1102.
- 681 THOMAS, LEIF N, TANDON, AMIT & MAHADEVAN, AMALA 2008 Submesoscale processes and dynamics.
682 *Ocean Modeling in an Eddying Regime, Geophys. Monogr. Ser* **177**, 17–38.
- 683 THOMAS, LEIF N., TAYLOR, JOHN R., FERRARI, RAFFAELE & JOYCE, T. M. 2013 Symmetric instability in the
684 Gulf Stream. *Deep Sea Research Part 2* **91**, 91–110.
- 685 THOMPSON, ANDREW F., LAZAR, AYAH, BUCKINGHAM, CHRISTIAN E., NAVEIRA GARABATO, ALBERTO C.,
686 DAMERELL, GILLIAN M. & HEYWOOD, KAREN J. 2016 Open-ocean submesoscale motions: A full
687 seasonal cycle of mixed layer instabilities from gliders. *J. Phys. Oceanogr.* .
- 688 TIMMERMANS, M-L., TOOLE, J., PROSHUTINSKY, A., KRISHFIELD, R. & PLUEDDEMANN, A. 2008 Eddies in the
689 Canada Basin, Arctic Ocean, observed from ice-tethered profilers. *Journal of Physical Oceanography*
690 **38** (1), 133–145.
- 691 WENEGRAT, JACOB O., CALLIES, J ORN & THOMAS, LEIF N. 2018 Submesoscale baroclinic instability in the
692 bottom boundary layer. *Journal of Physical Oceanography* **48** (11), 2571–2592.
- 693 YIM, EUNOK, STEGNER, ALEXANDRE & BILLANT, PAUL 2019 Stability criterion for the centrifugal instability
694 of surface intensified anticyclones. *Journal of Physical Oceanography* **49** (3), 827–849.
- 695 ZHAO, MENGAN, TIMMERMANS, MARY-LOUISE, COLE, SYLVIA, KRISHFIELD, RICHARD, PROSHUTINSKY,
696 ANDREY & TOOLE, JOHN 2014 Characterizing the eddy field in the Arctic Ocean halocline. *Journal*
697 *of Geophysical Research: Oceans* **119** (12), 8800–8817.